

# Encoding Cortical Surface by Spherical Harmonics

University of Wisconsin Madison, Department of Biostatistics  
and Medical Informatics Technical Report 198

Moo K. Chung<sup>1,2</sup>, Richard Hartley<sup>4</sup>, Kim Dalton<sup>2</sup>, Richard J. Davidson<sup>2,3</sup>

<sup>1</sup>*Department of Biostatistics and Medical Informatics*

<sup>2</sup>*Waisman Laboratory for Brain Imaging and Behavior*

<sup>3</sup>*Department of Psychology and Psychiatry*

*University of Wisconsin, Madison*

<sup>4</sup>*Department of Systems Engineering, Australian National University*

*Abstract:* There is a lack of unified statistical modeling framework for cerebral shape asymmetry analysis in literature. Most previous approaches start with flipping the 3D magnetic resonance images (MRI). The anatomical correspondence across the hemispheres is then established by registering the original image to the flipped image. A difference of an anatomical index between these two images is used as a measure of cerebral asymmetry. We present a radically different asymmetry analysis that utilizes a novel weighted spherical harmonic representation of cortical surfaces. The weighted spherical harmonic representation is a surface smoothing technique given explicitly as a weighted linear combination of spherical harmonics. This new representation is used to parameterize cortical surfaces, establish the hemispheric correspondence, and normalize cortical surfaces in a unified mathematical framework. The methodology has been applied in characterizing the cortical asymmetry of a group of autistic subjects.

*Key words and phrases:* Spherical Harmonics, Asymmetry Analysis, SPHARM, Cortical Surface, Heat Kernel

## 1. Introduction

Previous neuroanatomical studies have shown left occipital and right frontal lobe asymmetry, and left planum temporal asymmetry in normal controls (Barrick et al., 2005; Kennedy et al., 1999). These studies mainly flip the whole brain 3D MRI to obtain the mirror reflected MRI with respect to the mid-sagittal cross-section. Then the anatomical correspondence across the hemispheres is

established and a subsequent statistical analysis is performed at each voxel in the 3D MRI. Although this approach is sufficient for the voxel-based morphometry (Ashburner and Friston, 2000), where we only need an approximate alignment of corresponding brain substructures, it may fail to properly align highly convoluted sulcal and gyral foldings of gray matter. In order to address this shortcoming inherent in 3D whole brain volume asymmetry analysis, we need a new 2D cortical surface based framework.

The human cerebral cortex has the topology of a 2D highly convoluted grey matter shell of average thickness of 3mm. The outer boundary of the shell is called the *outer cortical surface* while the inner boundary is called the *inner cortical surface*. Cortical surfaces are segmented from magnetic resonance images (MRI) using a deformable surface algorithm and represented as a triangle mesh consisting of more than 40,000 vertices and 80,000 triangle elements (MacDonald et al., 2000; Chung et al., 2003) (Figure 1). We assume cortical surfaces to be smooth 2D Riemannian manifolds topologically equivalent to a unit sphere (Davatzikos and Bryan, 1995). A sample outer surface can be downloaded from <http://www.stat.wisc.edu/~mchung/software/hk/hk.html>. The detailed explanation on data loading, visualization and simple manipulation in MATLAB are given in the web link. The triangle mesh format contains information about vertex indices, the Cartesian coordinates of the vertices and the connectivity that tells which three vertices form a triangle. For any type of cortical surface mesh, if  $V$  is the number of vertices and  $E$  is the number of edges and  $F$  is the number of faces or triangles in the mesh, the Euler characteristic  $\chi$  of the mesh should be constant, i.e.  $\chi = V - E + F = 2$ . Note that for each triangle, there are 3 edges. Since two adjacent triangles share the same edge, the total number of edges is  $E = 3F/2$ . Hence, the relationship between the number of vertices and the triangles is  $F = 2V - 4$ . In the sample surface, we have 40,962 vertices and 81,920 triangles.

Once we obtain the both outer and inner cortical surfaces of a subject, *cortical thickness*, which is the distance between the outer and inner surfaces, is computed at each vertices of the outer surface (MacDonald et al., 2000). Since different clinical populations are expected to show different patterns of cortical thickness variations, cortical thickness has been used as a quantitative index

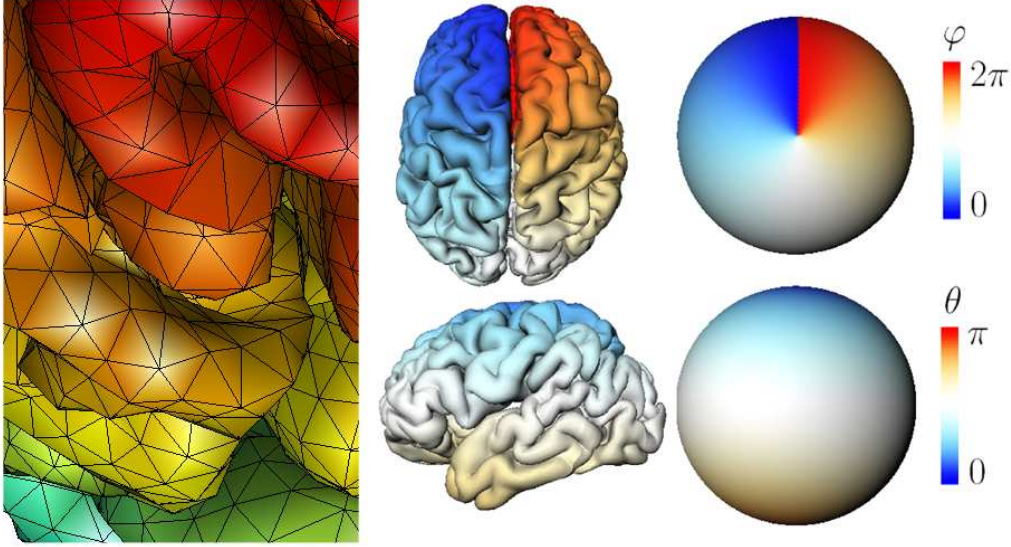


**Figure 1.** Left: The triangle mesh representation of the part of an outer cortical surface. The cortical thickness is measured at the vertices of the mesh. Right: Parameterization of cortical surface using the spherical coordinate system. The north and south poles are chosen in the plane, i.e.  $u_2 = 0$ , that separates the left and the right hemispheres.

for characterizing a clinical population (Chung et al., 2005). Cortical thickness varies locally by region and is likely to be influenced by aging, development and disease (Barta et al., 2005). By analyzing how cortical thickness differ locally in a clinical population with respect to a normal population, neuroscientists can locate the regions of abnormal anatomical differences in the clinical population. Cortical thickness serves as a metric of interest in performing 2D cortical asymmetry analysis. However, there are various methodological issues associated with using triangle mesh data. Our novel 2D surface modeling framework called the *weighted spherical harmonic representation* (Chung et al., 2007) can address these issues in a unified mathematical framework.

Cortical surface mesh construction and cortical thickness computation are expected to introduce noise. To counteract this, surface-based data smoothing is necessary. For 3D whole brain volume-based method, Gaussian kernel smoothing, which weights neighboring observations according to their 3D Euclidean distance, has been used. However, for data that lie on a 2D surface,

smoothing must be weighted according to the geodesic distance along the surface (Andrade et al., 2001; Chung et al., 2003). It will be shown that the weighted spherical harmonic representation is a 2D surface-based smoothing technique, where the explicit basis function expansion is used to smooth out noisy cortical surface data. The basis function expansion corresponds to the solution of isotropic heat diffusion. Unlike the previous surface based smoothing that solves the heat equation nonparametrically (Andrade et al., 2001; Cachia et al., 2003; Chung et al., 2003; Chung et al., 2005), the result of the weighted spherical harmonic representation is explicitly given as a weighted linear combination of spherical harmonics. This provides a more natural statistical modeling framework. A validation study showing the improved performance of the weighted spherical harmonic representation over heat kernel smoothing (Chung et al., 2005) will be given in the paper.

Comparing measurements defined at mesh vertices across different cortical surfaces is not a trivial task due to the fact no two cortical surfaces are identically shaped. In comparing measurements across different 3D whole brain images, 3D volume-based image registration is needed. However, 3D image registration techniques tend to misalign sulcal and gyral folding patterns of the cortex. Hence, 2D surface-based registration is needed in order to compare measurements across different cortical surfaces. Various surface registration methods have been proposed before (Thompson and Toga, 1996; Davatzikos, 1997; Miller et al., 1997; Fischl et al., 1999; Chung et al., 2005). These methods solve a complicated optimization problem of minimizing the measure of discrepancy between two surfaces. Unlike the previous computationally intensive methods, the weighted spherical harmonic representation provides a simple way of establishing surface correspondence between two surfaces in reducing the improper alignment of sulcal folding patterns without time consuming numerical optimization.

Once we establish surface correspondence between two surfaces, we also need to establish hemispheric correspondence within a subject for asymmetry analysis. However, it is not straightforward how to establish a 2D surface-based hemispheric correspondence. Although there are many 3D volume-based brain hemisphere asymmetry analysis (Barrick et al., 2005; Kennedy et al., 1999), due to this simple reason, there is a lack of 2D surface-based asymmetry analysis

in literature. This will be the first systematic study on 2D cortical asymmetry. The inherent angular symmetry presented in the weighted spherical harmonic representation can be used to establish the inter-hemispheric correspondence. It turns out that the usual asymmetry index of  $(L-R)/(L+R)$  is expressed as the ratio between the sum of positive and negative order harmonics.

The novelty of our proposed method is that surface parameterization, surface-based smoothing, within- and between- subject surface registration can be performed within a single unified mathematical framework providing a more consistent modeling framework than previously available for cortical analysis. This paper extends the five page conference paper (Chung et al., 2007) presented during the IEEE statistical signal processing workshop in 2007 with the detailed exposition of our methodology.

## 2. Methods

Cortical thickness is measured at each vertex and used as a measure for characterizing cortical shape variation. There exists a bijective mapping between the cortical surface  $\mathcal{M}$  and a unit sphere  $S^2$ , which is obtained via the deformable surface algorithm. Consider following parameterization of unit sphere  $S^2$ :

$$(u_1, u_2, u_3) = (\sin \theta \cos \varphi, \sin \theta \sin \varphi, \cos \theta)$$

with  $(\theta, \varphi) \in [0, \pi) \otimes [0, 2\pi)$ . The polar angle  $\theta$  is the angle from the north pole and the azimuthal angle  $\varphi$  is the angle along the horizontal cross-section. Then using the bijective mapping, we can parameterize the Cartesian coordinates  $v = (v_1, v_2, v_3)$  of each cortical mesh vertex in the cortical surface  $\mathcal{M}$  with the spherical angles  $(\theta, \varphi)$ , i.e.  $v = v(\theta, \varphi)$  (Figure 1). This enables us to represent cortical thickness measurements  $f$  with respect to the spherical coordinates, i.e.  $f = f(\theta, \varphi)$ . Each component of surface coordinates will be modeled independently as

$$v_i(\theta, \varphi) = h_i(\theta, \varphi) + \epsilon_i(\theta, \varphi), \tag{1}$$

where  $h_i$  is the unknown smooth coordinate function and  $\epsilon_i$  is zero mean random fields, possibly Gaussian. We also model cortical thickness  $f$  similarly as

$$f(\theta, \varphi) = g(\theta, \varphi) + e(\theta, \varphi),$$

where  $g$  is the unknown mean cortical thickness and  $e$  is a zero mean random field. We will further assume  $v_i, f \in \mathcal{L}^2(S^2)$ , the space of square integrable functions on unit sphere  $S^2$ . The unknown signals  $h_i$  and  $g$  are then estimated in the finite subspace of  $\mathcal{L}^2(S^2)$  spanned by harmonic basis functions in the least squares fashion.

### 2.1 Spherical Harmonics

The spherical harmonic  $Y_{lm}$  of degree  $l$  and order  $m$  is defined as

$$Y_{lm} = \begin{cases} c_{lm} P_l^{|m|}(\cos \theta) \sin(|m|\varphi), & -l \leq m \leq -1, \\ \frac{c_{lm}}{\sqrt{2}} P_l^{|m|}(\cos \theta), & m = 0, \\ c_{lm} P_l^{|m|}(\cos \theta) \cos(|m|\varphi), & 1 \leq m \leq l, \end{cases}$$

where  $c_{lm} = \sqrt{\frac{2l+1}{2\pi} \frac{(l-|m|)!}{(l+|m|)!}}$  and  $P_l^m$  is the *associated Legendre polynomial* of order  $m$  (Courant and Hilbert, 1953; Wahba, 1990). The associated Legendre polynomial is given by

$$P_l^m(x) = \frac{(1-x^2)^{m/2}}{2^l l!} \frac{d^{l+m}}{dx^{l+m}} (x^2-1)^l, x \in [-1, 1].$$

The first few terms of the spherical harmonics are

$$\begin{aligned} Y_{00} &= \frac{1}{\sqrt{4\pi}}, Y_{1,-1} = \sqrt{\frac{3}{4\pi}} \sin \theta \sin \varphi, \\ Y_{1,0} &= \sqrt{\frac{3}{4\pi}} \cos \theta, Y_{1,1} = \sqrt{\frac{3}{4\pi}} \sin \theta \cos \varphi. \end{aligned}$$

The spherical harmonics are orthonormal with respect to the inner product

$$\langle f_1, f_2 \rangle = \int_{S^2} f_1(\Omega) f_2(\Omega) d\mu(\Omega),$$

where  $\Omega = (\theta, \varphi)$  and the Lebesgue measure  $d\mu(\Omega) = \sin \theta d\theta d\varphi$ . The norm is then defined as

$$\|f_1\| = \langle f_1, f_1 \rangle^{1/2}. \quad (2)$$

Consider subspace  $\mathcal{I}_l$  spanned by the  $l$ -th degree spherical harmonics:

$$\mathcal{I}_l = \left\{ \sum_{m=-l}^l \beta_{lm} Y_{lm}(\Omega) : \beta_{lm} \in \mathbb{R} \right\}.$$

Then the subspace  $\mathcal{H}_k$  spanned by up to the  $k$ -th degree spherical harmonics is decomposed as the direct sum of  $\mathcal{I}_0, \dots, \mathcal{I}_k$ :

$$\begin{aligned}\mathcal{H}_k &= \mathcal{I}_0 \oplus \mathcal{I}_1 \cdots \oplus \mathcal{I}_k. \\ &= \left\{ \sum_{l=0}^k \sum_{m=-l}^l \beta_{lm} Y_{lm}(\Omega) : \beta_{lm} \in \mathbb{R} \right\}.\end{aligned}$$

Traditionally, the coordinate functions  $h_i$  are estimated by minimizing the integral of the squared residual within  $\mathcal{H}_k$ :

$$\hat{h}_i(\Omega) = \arg \min_{h \in \mathcal{H}_k} \int_{S^2} \left| v_i(\Omega) - h(\Omega) \right|^2 d\mu(\Omega). \quad (3)$$

It can be shown that the minimization is obtained when

$$\hat{h}_i(\Omega) = \sum_{l=0}^k \sum_{m=-l}^l \langle v_i, Y_{lm} \rangle Y_{lm}(\Omega). \quad (4)$$

Previously, representing anatomical boundary via the series expansion (4) is referred to as the *spherical harmonic representation* (Gerig et al., 2001; Gu et al., 2004; Shen et al., 2004; Shen and Chung, 2006). This technique has been used in representing hippocampus (Shen et al., 2004), ventricles (Gerig et al., 2001) and cortex (Gu et al., 2004; Shen and Chung, 2006).

## 2.2 Weighted Spherical Harmonic Representation

The weakness of the traditional spherical harmonic representation is that it produces the Gibbs phenomenon (ringing artifacts) (Gelb, 1997; Chung et al., 2007) for discontinuous and rapidly changing continuous measurements. The Gibbs phenomenon can be effectively removed if the spherical harmonic representation converges faster as the degree goes to infinity. By weighting the spherical harmonic coefficients exponentially smaller, we can make the representation converges faster. This can be achieved by additionally weighting the squared residuals in equation (3) with the *heat kernel*. Figure 2 demonstrate the severe Gibbs phenomenon in the traditional spherical harmonic representation (top row) on a hat shaped 2D surface. The hat shaped step function is simulated as  $z = 1$  for  $x^2 + y^2 < 1$  and  $z = 0$  for  $1 \leq x^2 + y^2 \leq 2$ . On the other hand the weighted spherical harmonic representation shows substantially reduced ringing artifacts. In both representations, we have used degree  $k = 42$ . For the weighted

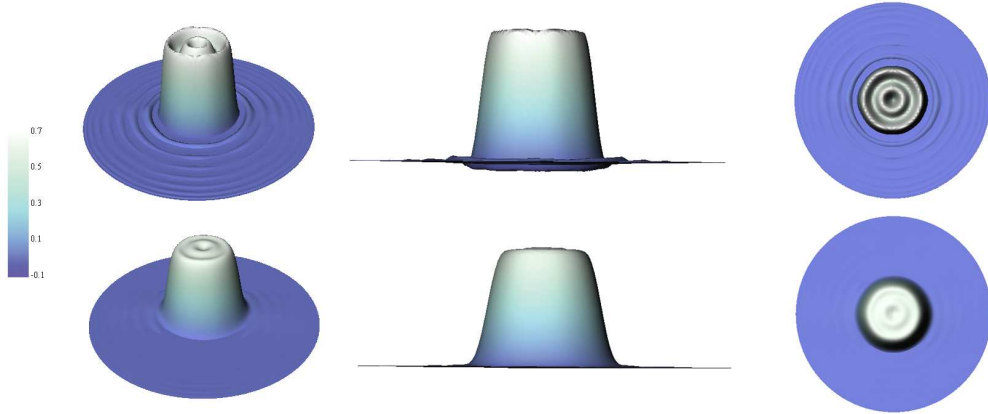


**Figure 2.** The Gibbs phenomenon on a hat shaped simulated surface showing the severe ringing effect on the traditional spherical harmonic representation (top) and reduced ringing effect on the weighted spherical harmonic representation (bottom). The degree  $k = 42$  is used for the both cases and bandwidth  $\sigma = 0.001$  is used for the weighted spherical harmonic representation.

spherical harmonic representation, the bandwidth  $\sigma = 0.001$  is used. This is the bandwidth we have used through the paper. Due to very complex folding patterns, sulcal regions of the brain exhibit more abrupt directional change than the simulated hat surface (upward of 180 degree compared to 90 degree in the hat surface) so there is a need for reducing the Gibbs phenomenon in the traditional spherical harmonic representation.

The heat kernel is the generalization of the Gaussian kernel defined in the Euclidean space to an arbitrary Riemannian manifold (Rosenberg, 1997; Chung et al., 2005). On a unit sphere, the heat kernel is written as

$$K_\sigma(\Omega, \Omega') = \sum_{l=0}^{\infty} \sum_{m=-l}^l e^{-l(l+1)\sigma} Y_{lm}(\Omega) Y_{lm}(\Omega'), \quad (5)$$

where  $\Omega = (\theta, \varphi)$  and  $\Omega' = (\theta', \varphi')$ . The heat kernel is symmetric and positive definite, and a probability distribution so that

$$\int_{S^2} K_\sigma(\Omega, \Omega') d\mu(\Omega) = 1.$$

The parameter  $\sigma$  controls the dispersion of the kernel so we will simply call it as the *bandwidth*. The heat kernel has the following asymptotic properties

$$\lim_{\sigma \rightarrow \infty} K_\sigma(\Omega, \Omega') = \frac{1}{4\pi}$$

and

$$\lim_{\sigma \rightarrow 0} K_\sigma(\Omega, \Omega') = \delta(\Omega - \Omega'),$$

the Dirac-delta function. The heat kernel can be further simplified using the harmonic addition theorem (Wahba, 1990) as

$$K_\sigma(\Omega, \Omega') = \sum_{l=0}^{\infty} \frac{2l+1}{4\pi} e^{-l(l+1)\sigma} P_l^0(\Omega \cdot \Omega'), \quad (6)$$

where  $\cdot$  is the Cartesian inner product.

Let us define *heat kernel smoothing* (Chung et al., 2005) as

$$K_\sigma * f(\Omega) = \int_{S^2} K(\Omega, \Omega') f(\Omega') d\mu(\Omega'). \quad (7)$$

Then the heat kernel smoothing has the following spectral representation, which can be easily seen by substituting (5) into equation (7) and rearranging the integral with the summation.

$$K_\sigma * f(\Omega) = \sum_{l=0}^{\infty} \sum_{m=-l}^l e^{-l(l+1)\sigma} \langle f, Y_{lm} \rangle Y_{lm}(\Omega), \quad (8)$$

The  $k$ -th degree finite series approximation of heat kernel smoothing will be referred to as the  *$k$ -th degree weighted spherical harmonic representation*. The unknown mean coordinates  $h_i$  are estimated using the weighted spherical harmonic representation, which is the minimizer of the of the weighted squared distance between measurements  $v_i$  and a function  $h$  in  $\mathcal{H}_k$  space. The unknown mean cortical thickness  $g$  is also estimated similarly.

**Theorem. 1**

$$\begin{aligned} & \sum_{l=0}^k \sum_{m=-l}^l e^{-l(l+1)\sigma} \langle v_i, Y_{lm} \rangle Y_{lm} \\ = & \arg \min_{h \in \mathcal{H}_k} \int_{S^2} \int_{S^2} K_\sigma(\Omega, \Omega') |v_i(\Omega') - h(\Omega)|^2 d\mu(\Omega') d\mu(\Omega) \end{aligned}$$

*Proof.* Let  $v_i = \sum_{l=0}^k \sum_{m=-l}^l \beta_{lm} Y_{lm}$ . Let the inner integral be

$$I = \int_{\mathcal{M}} K_\sigma(\Omega, \Omega') \left| v_i(\Omega') - \sum_{l=0}^k \sum_{m=-l}^l \beta_{lm} Y_{lm}(\Omega) \right|^2 d\mu(\Omega').$$

Simplifying the expression, we obtain,

$$\begin{aligned} I &= \sum_{l=0}^k \sum_{m=-l}^l \sum_{l'=0}^k \sum_{m'=-l'}^l 'Y_{lm}(\Omega) Y_{l'm'}(\Omega) \beta_{lm} \beta_{l'm'} \\ &\quad - 2K_\sigma * v_i(\Omega) \sum_{l=0}^k \sum_{m=-l}^l Y_{lm}(\Omega) \beta_{lm} + K * v_i^2(\Omega). \end{aligned}$$

Since  $I$  is an unconstrained positive semidefinite quadratic program (QP) in  $\beta_{lm}$ , there is no unique global minimizer of  $I$  without the additional linear constraints. Integrating  $I$  further with respect to  $\mu(\Omega)$ , we collapse the QP to a positive definite QP, which yields a unique global minimizer.

$$\int_{S^2} I d\mu(\Omega) = \sum_{l=0}^k \sum_{m=-l}^l \beta_{lm}^2 - 2 \sum_{i=0}^k e^{-l(l+1)\sigma} \langle v_i, Y_{lm} \rangle \beta_{lm} + \sum_{i=0}^{\infty} e^{-l(l+1)\sigma} \langle v_i^2, Y_{lm} \rangle$$

The minimum of the above integral is obtained when all the partial derivatives with respect to  $\beta_j$  vanishes.

$$\int_{S^2} \frac{\partial I}{\partial \beta_{lm}} d\mu(\Omega) = 2\beta_{lm} - 2e^{-l(l+1)\sigma} \langle v_i, Y_{lm} \rangle = 0.$$

Hence  $\sum_{l=0}^k \sum_{m=-l}^l e^{-l(l+1)\sigma} \langle v_i, Y_{lm} \rangle Y_{lm}$  is the unique minimizer in  $\mathcal{H}_k$ .

We can also show that the weighted spherical harmonic representation is related to previous available surface-based isotropic diffusion smoothing (Andrade et al., 2001; Cachia et al., 2003; Chung et al., 2003; Chung et al., 2005) via the following theorem.

**Theorem. 2.**

$$\sum_{l=0}^k \sum_{m=-l}^l e^{-l(l+1)\sigma} \langle v_i, Y_{lm} \rangle Y_{lm}(\Omega) = \arg \min_{h \in \mathcal{H}_k} \|h - h_0\|,$$

where  $h_0$  satisfies isotropic heat diffusion

$$\frac{\partial h_0}{\partial \sigma} = \Delta h_0 = \frac{1}{\sin \theta} \frac{\partial}{\partial \theta} \left( \sin \theta \frac{\partial h_0}{\partial \theta} \right) + \frac{1}{\sin^2 \theta} \frac{\partial^2 h_0}{\partial \varphi^2}, \quad (9)$$

with the initial value condition  $h_0(\Omega, \sigma = 0) = v_i(\Omega)$ .

*Proof.* We first prove that heat kernel smoothing (7) and its spectral representation (8) are the solution of the heat equation (9). At each fixed  $\sigma$ , which serves as the physical time of the heat equation, the solution  $h_0(\Omega, \sigma)$  belongs to  $\mathcal{L}^2(S^2)$ . So we can write the solution as

$$h_0(\Omega, \sigma) = \sum_{l=0}^{\infty} \sum_{m=-l}^l c_{lm}(\sigma) Y_{lm}(\Omega). \quad (10)$$

Since the spherical harmonics are the eigenfunctions of the spherical Laplacian (Wahba, 1990), we have

$$\Delta Y_{lm}(\Omega) = -l(l+1)Y_{lm}(\Omega). \quad (11)$$

Substituting equation (10) into equation (9) and using the relation (11), we obtain

$$\frac{\partial c_{lm}(\sigma)}{\partial \sigma} = -l(l+1)c_{lm}(\sigma). \quad (12)$$

The solution of the ordinary differential equation (12) is given by  $c_{lm}(\sigma) = b_{lm}e^{-l(l+1)\sigma}$  for some constant  $b_{lm}$ . Hence, we obtain the solution of the form

$$h_0(\Omega, \sigma) = \sum_{l=0}^{\infty} \sum_{m=-l}^l b_{lm}e^{-l(l+1)\sigma} Y_{lm}(\Omega).$$

When  $\sigma = 0$ , we have the initial condition

$$h_0(\Omega, 0) = \sum_{l=0}^{\infty} \sum_{m=-l}^l b_{lm} Y_{lm}(\Omega) = v_i(\Omega).$$

The coefficients  $b_{lm}$  must be the spherical harmonic coefficients, i.e.  $b_{lm} = \langle v_i, Y_{lm} \rangle$ . Then from the property of the generalized Fourier series (Rudin, 1991), the finite expansion is the closest to the infinite series in  $\mathcal{H}_k$ :

$$\sum_{l=0}^k \sum_{m=-l}^l e^{-l(l+1)\sigma} \langle v_i, Y_{lm} \rangle Y_{lm}(\Omega) = \arg \min_{h \in \mathcal{H}_k} \left\| h - h_0(\Omega, \sigma) \right\|.$$

This proves the statement of the theorem.

### 2.3 Estimating Spherical Harmonic Coefficients

The spherical harmonic coefficients are estimated based on an iterative procedure that utilizes the orthonormality of spherical harmonics. We assume that

coordinate functions are measured at  $n$  points  $\Omega_1, \dots, \Omega_n$ . Then we have the normal equations

$$v_i(\Omega_j) = \sum_{l=0}^k \sum_{m=-l}^l e^{-l(l+1)\sigma} \langle v_i, Y_{lm} \rangle Y_{lm}(\Omega_j), j = 1, \dots, n. \quad (13)$$

The normal equations (13) can be written in the matrix form as

$$\mathbf{V} = \underbrace{[\mathbf{Y}_0, e^{-1(1+1)\sigma} \mathbf{Y}_1, \dots, e^{-k(k+1)\sigma} \mathbf{Y}_k]}_{\mathbf{Y}} \beta, \quad (14)$$

where the column vectors are  $\mathbf{V} = [v_i(\Omega_1), \dots, v_i(\Omega_n)]'$  and  $\beta' = (\beta'_0, \beta'_1, \dots, \beta'_k)$  with  $\beta'_l = (\langle v_i, Y_{l,-l} \rangle, \dots, \langle v_i, Y_{l,l} \rangle)$ . The length of the vector  $\beta$  is

$$1 + (2 \cdot 1 + 1) + \dots + (2 \cdot k + 1) = (k + 1)^2.$$

Each submatrix  $\mathbf{Y}_l$  is given by

$$\mathbf{Y}_l = \begin{bmatrix} Y_{l,-l}(\Omega_1), & \dots, & Y_{l,l}(\Omega_1) \\ \vdots & \ddots & \vdots \\ Y_{l,-l}(\Omega_n), & \dots, & Y_{l,l}(\Omega_n) \end{bmatrix}.$$

We may tempted to directly estimate  $\beta$  in the least squares fashion as

$$\hat{\beta} = (\mathbf{Y}'\mathbf{Y})^{-1}\mathbf{Y}'\mathbf{V}.$$

However, for more than 40,000 mesh vertices we use in the study, the dimension of the design matrix is  $40,000 \times (k + 1)^2$ , which can easily reach the physical RAM memory limit of the most personal computers for large  $k$ . Instead of directly solving the huge normal equations, we project the normal equations into a smaller subspace  $\mathcal{I}_l$  and estimate  $2l + 1$  coefficients in an iterative fashion.

At degree 0, we write observations  $\mathbf{V}$  as

$$\mathbf{V} = \mathbf{Y}_0\beta_0 + \mathbf{r}_0,$$

where  $\mathbf{r}_0$  is the residual vector of estimating  $\mathbf{V}$  in subspace  $\mathcal{I}_0$ . Note that the residual vector  $\mathbf{r}_0$  consists of residual  $r_0(\Omega_j)$  at each point  $\Omega_j$ . Then we estimate  $\beta_0$  by minimizing the residual vector in a least squares fashion, i.e.

$$\hat{\beta}_0 = (\mathbf{Y}'_0\mathbf{Y}_0)^{-1}\mathbf{Y}'_0\mathbf{V} = \frac{\sum_{j=1}^n v_i(\Omega_j)Y_{00}(\Omega_j)}{\sum_{j=1}^n Y_{00}^2(\Omega_j)}.$$

At degree  $l$ , we have

$$\mathbf{r}_{l-1} = e^{-l(l+1)\sigma} \mathbf{Y}_l \beta_l + \mathbf{r}_l, \quad (15)$$

where the residual vector  $\mathbf{r}_{l-1}$  is obtained from the previous estimation

$$\mathbf{r}_{l-1} = \mathbf{V} - \mathbf{Y}_0 \hat{\beta}_0 \cdots - e^{-(l-1)l\sigma} \mathbf{Y}_{l-1} \hat{\beta}_{l-1}.$$

The least squares estimation of minimizing  $\mathbf{r}_l$  is then given by

$$\hat{\beta}_l = e^{l(l+1)\sigma} (\mathbf{Y}'_l \mathbf{Y}_l)^{-1} \mathbf{Y}'_l \mathbf{r}_{l-1}.$$

The correctness of the algorithm can be easily seen from the statement

$$\sum_{m=-l}^l e^{-l(l+1)\sigma} \langle v_i, Y_{lm} \rangle Y_{lm} = \arg \min_{h \in \mathcal{I}_l} \int_{S^2} K_\sigma(\Omega, \Omega') \left| r_{l-1}(\Omega') - h(\Omega) \right|^2 d\mu(\Omega'),$$

where the residual is given by

$$r_l(\Omega') = v_i(\Omega') - \sum_{l'=0}^l \sum_{m=-l'}^{l'} e^{-l(l+1)\sigma} \langle v_i, Y_{lm} \rangle Y_{lm}(\Omega').$$

This iterative algorithm is referred to as the *iterative residual fitting (IRF)* algorithm (Chung et al., 2007) since we are iteratively fitting a linear equation to the residuals obtained from the previous iteration. The IRF algorithm is similar to the *matching pursuit method* (Mallat and Zhang, 1993) although the IRF has been developed independently from the matching pursuit method. While the IRF algorithm was developed to avoid the computational burden of inverting a huge linear problem, the matching pursuit method was originally developed to compactly decompose a time frequency signal into a linear combination of pre-selected pool of basis functions. In the IRF algorithm, we minimize the residual component  $\mathbf{r}_l$  in the least squares fashion, i.e. minimizing the sum of squared residuals  $\sum_{j=1}^n r_l^2(\Omega_j)$  over all mesh vertices. On the other hand, in the marching pursuit method, the norm  $\|\mathbf{Y}_l \beta_l\|^2$  is maximized. Due to orthonormality, maximizing the norm is equivalent to minimizing the norm of the residual  $\|\mathbf{r}_l\|^2 = \int_{S^2} r_l^2(\Omega) d\mu(\Omega)$ . So there is a slight difference in how the residual is minimized. Although there is no limitation not to estimate multiple coefficients simultaneously in the matching pursuit method, Mallat and Zhang (1993) only

deals with the problem of estimating one coefficient at a time rather than multiple coefficients as in the IRF algorithm.

Although increasing the degree of the representation increases the goodness-of-fit, it also increases the number of estimated coefficients quadratically. So it is necessary to stop the iteration at the specific degree  $k$ , where the goodness-of-fit and the number of coefficients balance out. From equation (1), we can see that the  $k$ -th degree weighted spherical harmonic representation can be modeled as a linear model setting:

$$v_i(\Omega_j) = \sum_{l=0}^k \sum_{m=-l}^l e^{-l(l+1)\sigma} \beta_{lm}^i Y_{lm}(\Omega_j) + \epsilon_i(\Omega_j),$$

where the least squares estimation of  $\beta_{lm}^i$  is  $\widehat{\beta}_{lm}^i = \langle v_i, Y_{lm} \rangle$ . Then we stop the iteration at degree  $k$  by testing if the  $2k + 3$  coefficients at the next iteration vanishes:

$$H_0 : \beta_{k+1, -(k+1)}^i = \beta_{k+1, -k}^i = \dots = \beta_{k+1, k+1}^i = 0.$$

If we assume  $\epsilon_i$  to be a Gaussian random field, the usual  $F$  test at the significant level  $\alpha = 0.01$  can be used to determine the stopping degree. In our study, at bandwidth  $\sigma = 0.001$ , we stop the iteration at degree  $k = 42$ .

#### 2.4 Validation Against Heat Kernel Smoothing

The weighted spherical harmonic representation is validated against heat kernel smoothing as formulated in Chung et al. (2005). It is necessary to briefly explain how heat kernel smoothing is implemented in Chung et al. (2005). It was implemented as an iterated weighted averaging technique where the weights are spatially adapted to follow the shape of heat kernel in discrete fashion along a surface mesh. The algorithm has been implemented in MATLAB and it is freely available at <http://www.stat.wisc.edu/~mchung/software/hk/hk.html>. Since the introduction in 2005, the method has been used in smoothing various cortical surface data: cortical curvature (Luders et al., 2006; Gaser et al., 2006), cortical thickness (Luders et al., 2006), hippocampus (Shen et al., 2006; Zhu et al., 2007), magnetoencephalography (MEG) (Han et al., 2007) and functional-MRI (Hagler Jr., 2006; Jo et al., 2007).

Let us define the  $n$ -th iterated heat kernel smoothing of signal  $f \in L^2(S^2)$  as

$$K_\sigma^{(n)} * f(\Omega) = \underbrace{K_\sigma * \cdots * K_\sigma}_{n \text{ times}} * f(\Omega).$$

Then we have the following theorem

**Theorem. 3**

$$K_\sigma * f(\Omega) = K_{\sigma/n}^{(n)} * f(\Omega). \quad (16)$$

*Proof.* By letting  $f = Y_{l'm'}$  in equation (8) and using the orthonormality of spherical harmonics, we obtain

$$K_\sigma * Y_{l'm'}(\Omega) = \int_{S^2} K_\sigma(\Omega, \Omega') Y_{l'm'}(\Omega') d\mu(\Omega') = e^{-(l'+1)l'\sigma} Y_{l'm'}(\Omega).$$

This is the restatement of the fact that  $e^{-l(l+1)\sigma}$  and  $Y_{l'm'}$  are eigenvalues and eigenfunctions of the above integral equation with heat kernel. By reapplying heat kernel smoothing to equation (8), we obtain

$$K_\sigma^{(2)} * f(\Omega) = \sum_{l=0}^{\infty} \sum_{m=-l}^l e^{-l(l+1)\sigma} \langle f, Y_{lm} \rangle K_\sigma * Y_{lm}(\Omega) \quad (17)$$

$$= \sum_{l=0}^{\infty} \sum_{m=-l}^l e^{-l(l+1)2\sigma} \langle f, Y_{lm} \rangle Y_{lm}(\Omega). \quad (18)$$

Then arguing inductively we see obtain the spectral representation of the  $n$ -th iterated heat kernel smoothing

$$K_\sigma^{(n)} * f(\Omega) = \sum_{l=0}^{\infty} \sum_{m=-l}^l e^{-l(l+1)n\sigma} \langle f, Y_{lm} \rangle Y_{lm}(\Omega).$$

The right hand side is the spectral representation of heat kernel smoothing with bandwidth  $n\sigma$ . This proves

$$K_\sigma^{(n)} * f(\Omega) = K_{n\sigma} * f(\Omega).$$

By rescaling the bandwidth, we obtain the result.

Theorem 3 shows that heat kernel smoothing with large bandwidth  $\sigma$  can be decomposed into  $n$  repeated application of heat kernel smoothing with smaller

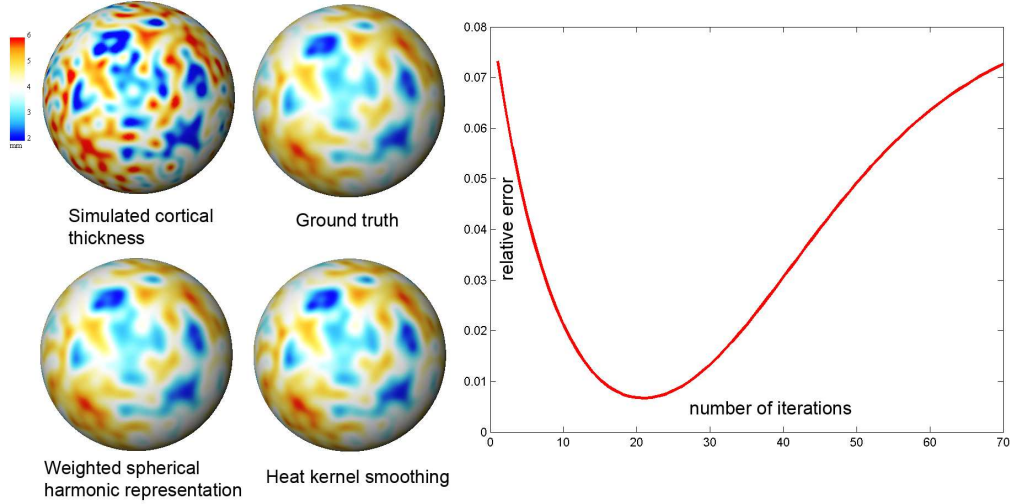


**Figure 3.** Cortical thickness is simulated from the sample cortical thickness. The ground truth is analytically constructed from the simulation. Then the weighted spherical harmonic representation and heat kernel smoothing of the simulated cortical thickness are compared against the ground truth. The plot is the relative error over the number of iterations for heat kernel smoothing against the ground truth.

bandwidth  $\sigma/n$ . When the bandwidth is small, heat kernel behaves like the Dirac-delta function and using the *parametrix expansion* (Rosenberg, 1997; Wang, 1997), we can approximate it locally using Gaussian kernel:

$$K_\sigma(\Omega, \Omega') = \frac{1}{\sqrt{4\pi\sigma}} \exp\left[-\frac{d^2(\Omega, \Omega')}{4\sigma}\right] [1 + O(\sigma^2)], \quad (19)$$

where  $d(p, q)$  is the geodesic distance between  $p$  and  $q$ . For small bandwidth, all the kernel weights are concentrated near the center so we only need to worry about the first neighbors of a given vertex in a surface mesh.

Let  $\Omega_1, \dots, \Omega_m$  be  $m$  neighboring vertices of vertex  $\Omega = \Omega_0$  in the mesh. The geodesic distance between  $\Omega$  and its adjacent vertex  $\Omega_i$  is the length of edge between these two vertices in the mesh. Then the discretized and normalized heat kernel is given by

$$W_\sigma(\Omega, \Omega_i) = \frac{\exp\left(-\frac{d(\Omega, \Omega_i)^2}{4\sigma}\right)}{\sum_{j=0}^m \exp\left(-\frac{d(\Omega, \Omega_j)^2}{4\sigma}\right)}.$$

Note that  $\sum_{i=0}^m W_\sigma(\Omega, \Omega_i) = 1$ . The discrete version of heat kernel smoothing on a triangle mesh is then defined as

$$W_\sigma * f(\Omega) = \sum_{i=0}^m W_\sigma(\Omega, \Omega_i) f(\Omega_i).$$

The discrete kernel smoothing should converges to heat kernel smoothing (7) as the mesh resolution increases. This is the form of *Nadaraya-Watson estimator* (Chaudhuri and Marron, 2000) applied to surface data. Instead of performing a single kernel smoothing with large bandwidth  $n\sigma$ , we perform  $n$  iterated kernel smoothing with small bandwidth  $\sigma$  as follows  $W_\sigma^{(n)} * f(\Omega)$ .

For comparison between the weighted spherical harmonic representation and heat kernel smoothing, we have used the sample cortical thickness data in constructing the analytical ground truth. Consider a surface measurement of the form

$$f(\Omega) = \sum_{l=0}^k \sum_{m=-l}^l \beta_{lm} Y_{lm}(\Omega) \quad (20)$$

for some given  $\beta_{lm}$ . Heat kernel smoothing of  $f$  is given as an exact analytic form, which serves as the ground truth for validation:

$$K_\sigma * f(\Omega) = \sum_{l=0}^k \sum_{m=-l}^l e^{-l(l+1)\sigma} \beta_{lm} Y_{lm}(\Omega). \quad (21)$$

Using the sample cortical thickness data, we simulated the measurement of the form (20) by estimating  $\beta_{lm} = \langle f, Y_{lm} \rangle$  (Figure 3 top left). Then we have compared the weighted spherical harmonic representation of  $f$  and the discrete version of heat kernel smoothing  $W_{\sigma/n}^{(n)} * f$  against the the analytical ground truth (21) (Figure 3 top right) along the surface mesh.

For the weighted spherical harmonic representation, we have used  $\sigma = 0.001$  and the corresponding optimal degree  $k = 42$  (Figure 3 bottom left). The relative error for the weighted spherical harmonic representation is up to 0.013 at a certain vertex and the mean relative error over all mesh vertices is 0.0012. For heat kernel smoothing, we have used varying number of iterations  $1 \leq n \leq 70$  and the corresponding bandwidth  $\sigma = 0.001/n$ . The performance of heat kernel smoothing depends on the number of iterations as shown in the plot of relative

error over the number of iterations in Figure 3. The minimum relative error is obtained when 21 iterations are used (Figure 3 bottom right). The relative error is up to 0.055 and the mean relative error is 0.0067. Our simulation result demonstrates the weighted spherical harmonic representation performs better than heat kernel smoothing. The main problem with heat kernel smoothing is that the number of iterations need to be predetermined possibly using the proposed simulation technique. Even at the optimal iteration of 21, the weighted spherical harmonic representation provides a better performance.

### 2.5 Encoding Surface Asymmetry Information

Given the weighted spherical harmonic representation, we need to establish surface correspondence between hemispheres and between subjects. This requires establishing anatomical correspondence using *surface registration*. The main motivation for the surface registration is to establish proper alignment for cortical thickness to be compared across subjects and between hemispheres. Previously, the cortical surface registration was performed by minimizing an objective function that measures the global fit of two surfaces while maximizing the smoothness of the deformation in such a way that the sulcal and gyral folding patterns are matched smoothly (Thompson and Toga, 1996; Robbins, 2003; Chung et al., 2005). In the weighted spherical harmonic representation, surface registration is straightforward and does not require any sort of time consuming optimization explicitly. Consider a surface  $\hat{h}_i$  obtained from coordinate functions  $v_i$  measured at points  $\Omega_1, \dots, \Omega_n$ :

$$\hat{h}_i(\Omega) = \sum_{l=0}^k \sum_{m=-l}^l e^{-l(l+1)\sigma} \langle v_i, Y_{lm} \rangle(\Omega).$$

Consider the other surface  $\hat{j}_i$  obtained from coordinate functions  $w_i$  measured at points  $\Omega'_1, \dots, \Omega'_m$ :

$$\hat{j}_i(\Omega) = \sum_{l=0}^k \sum_{m=-l}^l e^{-l(l+1)\sigma} \langle w_i, Y_{lm} \rangle(\Omega).$$

Suppose the surface  $\hat{h}_i$  is deformed to  $\hat{h}_i + d_i(\hat{h}_i)$  under the influence of the displacement vector field  $d_i$ . We wish to find  $d_i$  that minimizes the discrepancy between  $\hat{h}_i + d_i(\hat{h}_i)$  and  $\hat{j}_i$  in the finite subspace  $\mathcal{H}_k$ . This can be easily done by noting that

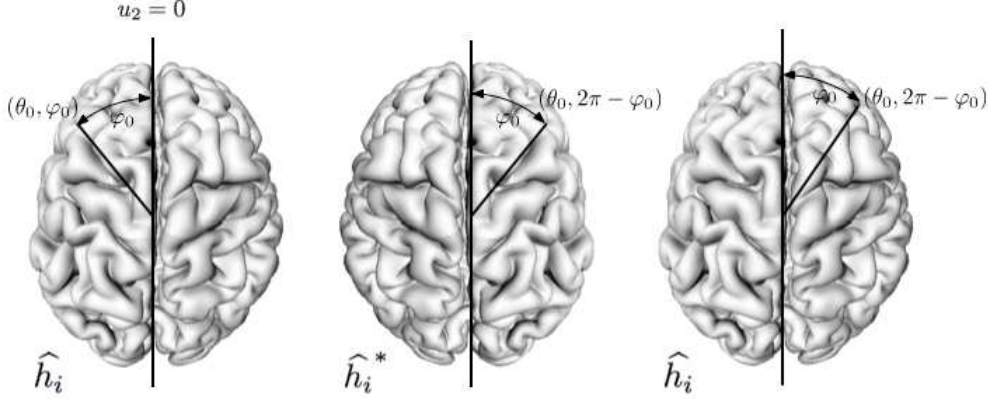


**Figure 4.** The point  $\widehat{h}_i(\theta_0, \varphi_0)$  (left) corresponds to  $\widehat{h}_i^*(\theta, 2\pi - \varphi_0)$  (middle) after mirror reflection with respect to the midsagittal cross section  $u_2 = 0$ . From the spherical harmonic correspondence,  $\widehat{h}_i^*(\theta, 2\pi - \varphi_0)$  corresponds to  $\widehat{h}_i(\theta, 2\pi - \varphi_0)$  (right). This establish the mapping from the left hemisphere to the right hemisphere in the least squares fashion.

$$\sum_{l=0}^k \sum_{m=-l}^l e^{-l(l+1)\sigma} (w_{lm}^i - v_{lm}^i) Y_{lm}(\Omega) = \arg \min_{d_i \in \mathcal{H}_k} \left\| \widehat{h}_i + d_i(\widehat{h}_i) - \widehat{j}_i \right\|. \quad (22)$$

The proof of this statement is given in Chung et al. (2007). This implies that the optimal displacement in the least squares sense is obtained by simply taking the difference between two weighted spherical harmonic representation and matching coefficients of the same degree and order. Then a specific point  $\widehat{h}_i(\Omega_0)$  in one surface corresponds to  $\widehat{j}_i(\Omega_0)$  in the other surface. We will refer this point-to-point surface correspondence as the *spherical harmonic correspondence*.

The spherical harmonic correspondence can be further used to establish the inter-hemispheric correspondence by letting  $\widehat{j}_i$  to be the mirror reflection of  $\widehat{h}_i$ . The mirror reflection of  $\widehat{h}_i$  with respect to the midsagittal cross section  $u_2 = 0$  is simply given by

$$\widehat{j}_i(\theta, \varphi) = \widehat{h}_i^*(\theta, \varphi) = \widehat{h}_i(\theta, 2\pi - \varphi),$$

where  $*$  denotes the mirror reflection operation (Figure 4). The specific point  $\widehat{h}_i(\theta_0, \varphi_0)$  in the left hemisphere will be mirror reflected to  $\widehat{j}_i(\theta_0, 2\pi - \varphi_0)$  in the

right hemisphere. The spherical harmonic correspondence of  $\widehat{j}_i(\theta_0, 2\pi - \varphi_0)$  is  $\widehat{h}_i(\theta_0, 2\pi - \varphi_0)$ . Hence, the point  $\widehat{h}_i(\theta_0, \varphi_0)$  in the left hemisphere corresponds to the point  $\widehat{h}_i(\theta_0, 2\pi - \varphi_0)$  in the right hemisphere. This establishes the inter-hemispheric anatomical correspondence. The schematics of obtaining this inter-hemispheric correspondence is given in Figure 4. This inter-hemispheric correspondence is used to compare cortical thickness measurements  $f$  across the hemispheres. The weighted spherical harmonic representation of cortical thickness  $f$  is given by

$$\widehat{g}(\theta, \varphi) = \sum_{l=0}^k \sum_{m=-l}^l e^{-l(l+1)\sigma} \langle f, Y_{lm} \rangle Y_{lm}(\theta, \varphi).$$

At a given position  $h_i(\theta_0, \varphi_0)$ , the corresponding cortical thickness is  $\widehat{g}(\theta_0, \varphi_0)$ , which should be compared with the thickness  $\widehat{g}(\theta_0, 2\pi - \varphi_0)$  at position  $\widehat{h}_i(\theta_0, 2\pi - \varphi_0)$ :

$$\widehat{g}(\theta_0, 2\pi - \varphi_0) = \sum_{l=0}^k \sum_{m=-l}^l e^{-l(l+1)\sigma} \langle f, Y_{lm} \rangle Y_{lm}(\theta_0, 2\pi - \varphi_0). \quad (23)$$

The equation (23) can be rewritten using the property of spherical harmonics:

$$Y_{lm}(\theta, 2\pi - \varphi) = \begin{cases} -Y_{lm}(\theta, \varphi), & -l \leq m \leq -1, \\ Y_{lm}(\theta, \varphi), & 0 \leq m \leq l. \end{cases}$$

$$\begin{aligned} \widehat{g}(\theta_0, 2\pi - \varphi_0) &= \sum_{l=0}^k \sum_{m=-l}^{-1} e^{-l(l+1)\sigma} \langle f, Y_{lm} \rangle Y_{lm}(\theta_0, \varphi_0) \\ &\quad - \sum_{l=0}^k \sum_{m=0}^l e^{-l(l+1)\sigma} \langle f, Y_{lm} \rangle Y_{lm}(\theta_0, \varphi_0). \end{aligned}$$

Comparing with the expansion for  $\widehat{g}(\theta_0, \varphi_0)$ , we see that the negative order terms are invariant while the positive order terms change the sign. Hence we define the *symmetry index* as

$$S(\theta, \varphi) = \frac{1}{2} \left[ \widehat{g}(\theta, \varphi) + \widehat{g}(\theta, 2\pi - \varphi) \right] = \sum_{l=0}^k \sum_{m=-l}^{-1} e^{-l(l+1)\sigma} \langle f, Y_{lm} \rangle Y_{lm}(\theta_0, \varphi_0)$$

while the *asymmetry index* as

$$A(\theta, \varphi) = \frac{1}{2} \left[ \widehat{g}(\theta, \varphi) - \widehat{g}(\theta, 2\pi - \varphi) \right] = \sum_{l=0}^k \sum_{m=0}^l e^{-l(l+1)\sigma} \langle f, Y_{lm} \rangle Y_{lm}(\theta_0, \varphi_0).$$

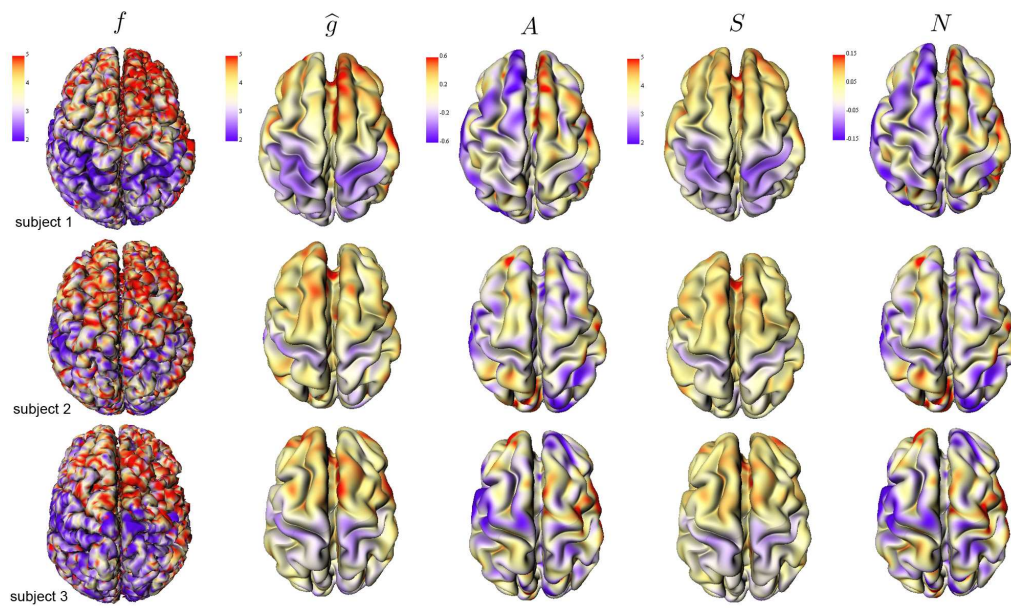


**Figure 5.** Three representative subjects showing cortical thickness ( $f$ ), its weighted-SPHARM representation ( $\hat{g}$ ), asymmetry index ( $A$ ), symmetry index ( $S$ ) and normalized asymmetry index ( $N$ ). The Cortical thickness is projected onto the original brain surfaces while all other measurements are projected onto the 42-th degree weighed spherical harmonic representation

We normalize the asymmetry index by dividing the asymmetry index by the symmetry index as

$$N(\theta, \varphi) = \frac{\widehat{g}(\theta, \varphi) - \widehat{g}(\theta, 2\pi - \varphi)}{\widehat{g}(\theta, \varphi) + \widehat{g}(\theta, 2\pi - \varphi)} = \frac{\sum_{l=1}^k \sum_{m=-l}^{-1} e^{-l(l+1)\sigma} \langle f, Y_{lm} \rangle Y_{lm}(\theta, \varphi)}{\sum_{l=0}^k \sum_{m=0}^l e^{-l(l+1)\sigma} \langle f, Y_{lm} \rangle Y_{lm}(\theta, \varphi)}.$$

We will refer this index to as the *normalized asymmetry index*. The numerator is the sum of all negative orders while the denominator is the sum of all positive and the 0-th orders. Note that  $N(\theta, 0) = N(\theta, \pi) = 0$ . This index is intuitively interpreted as the normalized difference between cortical thickness in the left and the right hemispheres. Note that the larger the value of the index, the larger the amount of asymmetry. The index is invariant under the affine scaling of the human brain so it is not necessary to control for the global brain size difference in the later statistical analysis. Figure 5 shows the asymmetry index for 3 selective subjects.

### 3. Application to Autism Study

#### 3.1 Description of Data Set

Three Tesla  $T_1$ -weighted MR scans were acquired for 16 high functioning autistic and 12 control right handed males. The autistic subjects were diagnosed by a trained and certified psychologist at the Waisman center at the University of Wisconsin-Madison (Dalton et al., 2005). The average ages are  $17.1 \pm 2.8$  and  $16.1 \pm 4.5$  for control and autistic groups respectively. Image intensity nonuniformity was corrected using a nonparametric nonuniform intensity normalization method (Sled et al., 1988) and then the image was spatially normalized into the Montreal neurological institute stereotaxic space using a global affine transformation (Collins et al., 1994). Afterwards, an automatic tissue-segmentation algorithm based on a supervised artificial neural network classifier was used to segment gray and white matters (Kollakian, 1996). Triangle meshes for outer cortical surfaces were obtained by a deformable surface algorithm (MacDonald et al., 2000) and the mesh vertex coordinates  $v_i$  are obtained. At each vertex, cortical thickness  $f$  is also measured. Once we obtained the outer cortical surfaces of 28 subjects, the weighted spherical harmonic representations  $\widehat{h}_i$  are constructed. We have used bandwidth  $\sigma = 0.001$  corresponding to  $k = 42$  degrees. The weighted spherical harmonic representation for three representative subjects are given in

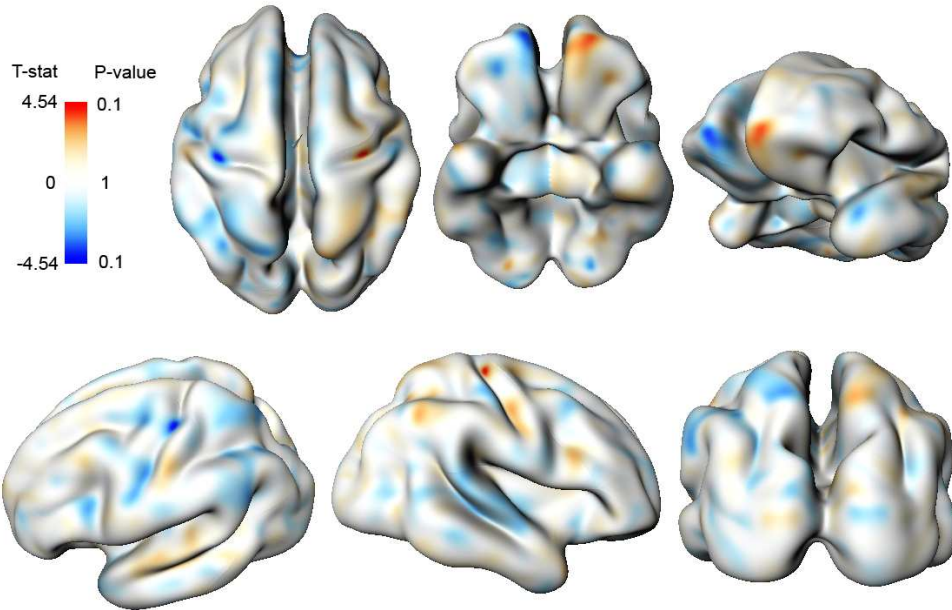


**Figure 6.** The statistically significant regions of cortical asymmetry thresholded at the corrected P-value of 0.1. The P-value has been corrected for multiple comparisons.

Figure 5. The symmetry ( $S$ ), asymmetry ( $A$ ) and normalized asymmetry ( $N$ ) indices are computed. The normalized asymmetry index is used in localizing the regions of cortical asymmetry difference between two groups. These indices are projected on the average cortical surface (Figure 5). The average cortical surface is constructed by averaging the Fourier coefficients of all subjects within the same spherical harmonics basis following the spherical harmonic correspondence. The average surface serves as an anatomical landmark for displaying these indices as well as projecting the final statistical analysis results in the next section.

### 3.2 Statistical Inference on Surface Asymmetry

For each subject, its normalized asymmetry index  $A(\theta, \varphi)$  is computed and modeled as a Gaussian random field. The null hypothesis is that  $A(\theta, \varphi)$  is identical to the both groups for all  $(\theta, \varphi)$  while the alternate hypothesis is that there is a specific point  $(\theta_0, \varphi_0)$ , at which the normalized asymmetry index is different for the both groups. The group difference on the normalized asymmetry index

is tested using the  $T$  random field, denoted as  $T(\theta, \varphi)$ . Since we need to perform the test on every points on the cortical surface, it becomes a multiple comparison problem. We used the random field theory based  $t$  statistic thresholding to determine the statistical significance (Worsley et al., 1996). The probability of obtaining false positives for the one sided alternate hypothesis is given from the following formula:

$$P\left[\sup_{(\theta, \varphi) \in S^2} T(\theta, \varphi) > h\right] \approx \sum_{d=0}^2 R_d(S^2) \mu_d(h), \quad (24)$$

where  $R_d$  is the  $d$ -dimensional *Resels* of  $S^2$  and  $\rho_d$  is the  $d$ -dimensional *Euler characteristic (EC) density* of  $T$ -field (Worsley et al., 1996; Worsley et al., 2004). The Resels are

$$R_0(S^2) = 2, R_1(S^2) = 0, R_2(S^2) = \frac{4\pi}{\text{FWHM}^2},$$

where FWHM is the *full width at the half maximum* of smoothing kernel. The FWHM of heat kernel used in the weighted spherical harmonic representation is not given in a close form, so it is computed numerically. From equation (6), the maximum of the heat kernel is obtained when  $\Omega \cdot \Omega' = 1$ . Then we numerically solve for  $\Omega \cdot \Omega'$ :

$$\frac{1}{2} \sum_{l=0}^k \frac{2l+1}{4\pi} e^{-l(l+1)\sigma} = \sum_{l=0}^k \frac{2l+1}{4\pi} e^{-l(l+1)\sigma} P_l^0(\Omega \cdot \Omega').$$

In previous surface data smoothing techniques (Chung et al., 2003; Chung et al., 2005), FWHM of between 20 to 30 mm is used for smoothing data directly along the brain surface. In our study, we use substantially smaller FWHM since the analysis is performed on the unit sphere which has smaller surface area. The compatible Resels of the unit sphere can be obtained by using the bandwidth of  $\sigma = 0.001$ , which corresponds to the FWHM of 0.0968 mm. Then based on the formula (24), we computed the multiple comparison corrected P-value and thresholded at  $\alpha = 0.1$  (Figure 6). We found that the central sulci and the prefrontal cortex exhibits abnormal cortical asymmetry pattern in autistic subjects. The larger positive  $t$  statistic value indicates thicker cortical thickness with respect to the corresponding thickness at the opposite hemisphere.

#### 4. Conclusions

We have presented a novel cortical asymmetry technique called the weighted spherical harmonic representation that unifies surface representation, parameterization, smoothing and registration in a unified mathematical framework. The weighed spherical representation is formulated as the least squares approximation to an isotropic heat diffusion on a unit sphere in such a way that the physical time of heat diffusion controls the amount of smoothing in the weighted spherical harmonic representation. The methodology is used in modeling cortical surface shape asymmetry. Within this framework, the asymmetry index that measures the amount of asymmetry presented in the cortical surface, was constructed as the ratio of the weighted spherical harmonic representation of negative and positive orders. The regions of statistically different asymmetry index was localized using the random field theory. As an illustration, the methodology was applied quantifying the abnormal cortical asymmetry pattern of autistic subjects. The weighted spherical harmonic representation is a very general surface shape representation so it can be used for any type of surface objects that are topologically equivalent to a unit sphere.

#### REFERENCES

- Andrade, A., Kherif, F., Mangin, J., Worsley, K., Paradis, A., Simon, O., Dehaene, S., Le Bihan, D. and Poline, J.-B. (2001). Detection of fmri activation using cortical surface mapping. *Human Brain Mapping* **12**, 79–93.
- Ashburner, J. and Friston, K. (2000). Voxel-based morphometry - the methods. *NeuroImage* **11**, 805–821.
- Barrick, T., Mackay, C., Prima, S., maes, F., Vandermeulen, D., Crow, T. and Roberts, N. (2005). Automatic analysis of cerebral asymmetry: an exploratory study of the relationship between brain torque and planum temporale asymmetry. *NeuroImage* **24**, 678–691.
- Barta, P., Miller, M. and Qiu, A. (2005). A stochastic model for studying the laminar structure of cortex from mri. *IEEE Transactions on Medical Imaging* **24**, 728–742.
- Cachia, A., Mangin, J.-F., D., R., Papadopoulos-Orfanos, D., Kherif, F., Bloch,

- I. and Régis, J. (2003). A generic framework for parcellation of the cortical surface into gyri using geodesic voronoï diagrams. *Image Analysis* **7**, 403–416.
- Chaudhuri, P. and Marron, J. S. (2000). Scale space view of curve estimation. *The Annals of Statistics* **28**, 408–428.
- Chung, M., Dalton, K. and Davidson, R. (2007). Encoding neuroanatomical information using weighted spherical harmonic representation. In *IEEE Signal Processing Workshop*.
- Chung, M., Dalton, K.M., S. L., Evans, A. and Davidson, R. (2007). Weighted fourier representation and its application to quantifying the amount of gray matter. *IEEE transactions on medical imaging* **26**, 566–581.
- Chung, M., Robbins, S., Dalton, K.M., D. R. A. A. and Evans, A. (2005). Cortical thickness analysis in autism with heat kernel smoothing. *NeuroImage* **25**, 1256–1265.
- Chung, M., Worsley, K., Robbins, S., Paus, T., Taylor, J., Giedd, J., Rapoport, J. and Evans, A. (2003). Deformation-based surface morphometry applied to gray matter deformation. *NeuroImage* **18**, 198–213.
- Collins, D., Neelin, P., Peters, T. and Evans, A. (1994). Automatic 3d inter-subject registration of mr volumetric data in standardized talairach space. *J. Comput. Assisted Tomogr.* **18**, 192–205.
- Courant, R. and Hilbert, D. (1953). *Methods of Mathematical Physics: Volume II*. Interscience, New York, english edition.
- Dalton, K., Nacewicz, B., Johnstone, T., Schaefer, H., Gernsbacher, M., Goldsmith, H., Alexander, A. and Davidson, R. (2005). Gaze fixation and the neural circuitry of face processing in autism. *Nature Neuroscience* **8**, 519–526.
- Davatzikos, C. (1997). Spatial transformation and registration of brain images using elastically deformable models. *Comput. Vis. Image Underst.* **66**, 207–222.
- Davatzikos, C. and Bryan, R. (1995). Using a deformable surface model to obtain a shape representation of the cortex. *Proceedings of the IEEE International Conference on Computer Vision* **9**, 2122–2127.
- Fischl, B., Sereno, M., Tootell, R. and Dale, A. (1999). High-resolution intersubject averaging and a coordinate system for the cortical surface. *Hum. Brain Mapping* **8**, 272–284.

- Gaser, C., Luders, E., Thompson, P., Lee, A., Dutton, R., Geaga, J., Hayashi, K., Bellugi, U., Galaburda, A., Korenberg, J., Mills, D., Toga, A. and Reiss, A. (2006). Increased local gyrification mapped in williams syndrome. *NeuroImage* **33**, 46–54.
- Gelb, A. (1997). The resolution of the gibbs phenomenon for spherical harmonics. *Mathematics of Computation* **66**, 699–717.
- Gerig, G., Styner, M., Jones, D., Weinberger, D. and Lieberman, J. (2001). Shape analysis of brain ventricles using spharm. In *MMBIA*, pages 171–178.
- Gu, X., Wang, Y., Chan, T., Thompson, T. and S.T., Y. (2004). Genus zero surface conformal mapping and its application to brain surface mapping. *IEEE Transactions on Medical Imaging* **23**, 1–10.
- Hagler Jr., D.J., S. A. S. M. (2006). Smoothing and cluster thresholding for cortical surface-based group analysis of fmri data. *NeuroImage* **33**, 1093–1103.
- Han, J., Kim, J., Chung, C. and Park, K. (2007). Evaluation of smoothing in an iterative lp-norm minimization algorithm for surface-based source localization of meg. *Physics in Medicine and Biology* **52**, 4791–4803.
- Jo, H., Lee, J.-M., Kim, J.-H., Shin, Y.-W., Kim, I.-Y., Kwon, J. and Kim, S. (2007). Spatial accuracy of fmri activation influenced by volume- and surface-based spatial smoothing techniques. *NeuroImage* **34**, 550–564.
- Kennedy, D., O’Craven, K., Ticho, B., Goldstein, A., Makris, N. and Henson, J. (1999). Structural and functional brain asymmetries in human situs inversus totalis. *Neurology* **53**, 1260–1265.
- Kollakian, K. (1996). Performance analysis of automatic techniques for tissue classification in magnetic resonance images of the human brain. Technical Report Master’s thesis, Concordia University, Montreal, Quebec, Canada.
- Luders, E., Narr, K., Thompson, P., Rex, D., Woods, R. and DeLuca, H., J. L. a. A. (2006). Gender effects on cortical thickness and the influence of scaling. *Human Brain Mapping* **27**, 314–324.
- Luders, E., Thompson, P.M., Narr, K., Toga, A., Jancke, L. and Gaser, C. (2006). A curvature-based approach to estimate local gyrification on the cortical surface. *NeuroImage* **29**, 1224–1230.
- MacDonald, J., Kabani, N., Avis, D. and Evans, A. (2000). Automated 3-d extraction of inner and outer surfaces of cerebral cortex from mri. *NeuroImage*

- 12, 340–356.
- Mallat, S. and Zhang, Z. (1993). Matching pursuits with time-frequency dictionaries. *IEEE Transactions on Signal Processing* **41**, 3397–3415.
- Miller, M., Banerjee, A., Christensen, G., Joshi, S., Khaneja, N., Grenander, U. and Matejic, L. (1997). Statistical methods in computational anatomy. *Statistical Methods in Medical Research* **6**, 267–299.
- Robbins, S. (2003). Anatomical standardization of the human brain in euclidean 3-space and on the cortical 2-manifold. Technical Report PhD thesis, School of Computer Science, McGill University, Montreal, Quebec, Canada.
- Rosenberg, S. (1997). *The Laplacian on a Riemannian Manifold*. Cambridge University Press.
- Rudin, W. (1991). *Functional Analysis*. McGraw-Hill.
- Shen, L. and Chung, M. (2006). Large-scale modeling of parametric surfaces using spherical harmonics. In *Third International Symposium on 3D Data Processing, Visualization and Transmission (3DPVT)*.
- Shen, L., Ford, J., Makedon, F. and Saykin, A. (2004). surface-based approach for classification of 3d neuroanatomical structures. *Intelligent Data Analysis* **8**, 519–542.
- Shen, L., Saykin, A., Chung, M., Huang, H., Ford, J., Makedon, F., McHugh, T. and Rhodes, C. (2006). Morphometric analysis of genetic variation in hippocampal shape in mild cognitive impairment: Role of an il-6 promoter polymorphism. In *Life Science Society Computational Systems Bioinformatics Conference*.
- Sled, J., Zijdenbos, A. and Evans, A. (1988). A nonparametric method for automatic correction of intensity nonuniformity in mri data. *IEEE Transactions on Medical Imaging* **17**, 87–97.
- Thompson, P. and Toga, A. (1996). A surface-based technique for warping 3-dimensional images of the brain. *IEEE Transactions on Medical Imaging* **15**.
- Wahba, G. (1990). *Spline models for observational data*. SIAM.
- Wang, F.-Y. (1997). Sharp explicit lower bounds of heat kernels. *Annals of Probability* **24**, 1995–2006.
- Worsley, K., Marrett, S., Neelin, P., Vandal, A., Friston, K. and Evans, A. (1996). A unified statistical approach for determining significant signals in images of

- cerebral activation. *Human Brain Mapping* **4**, 58–73.
- Worsley, K., Taylor, J., Tomaiuolo, F. and Lerch, J. (2004). Unified univariate and multivariate random field theory. *NeuroImage* **23**, S189–195.
- Zhu, H., Ibrahim, J., Tang, N., Rowe, D., Hao, X., Bansal, R. and Peterson, B. (2007). A statistical analysis of brain morphology using wild bootstrapping. *IEEE Transactions on Medical Imaging* **26**, 954–966.